A New Method to Reduce Truncation Errors in Partial Spherical Near-Field Measurements

F. J. Cano-Fácila[1], S. Pivnenko[2]

[1]*Radiation Group; Signals, Systems and Radiocommunications Department; Technical University of Madrid*
Ciudad Universitaria, 28040 Madrid, Spain
francisco@gr.ssr.upm.es

[2] *Department of Electrical Engineering; Technical University of Denmark*
DK-2800 Kgs. Lyngby, Denmark
sp@elektro.dtu.dk

***Abstract*— A new and effective method for reduction of truncation errors in partial spherical near-field (SNF) measurements is proposed. The method is useful when measuring electrically large antennas, where the measurement time with the classical SNF technique is prohibitively long and an acquisition over the whole spherical surface is not practical. Therefore, to reduce the data acquisition time, partial sphere measurement is usually made, taking samples over a portion of the spherical surface in the direction of the main beam. But in this case, the radiation pattern is not known outside the measured angular sector as well as a truncation error is present in the calculated far-field pattern within this sector. The method is based on the Gerchberg-Papoulis algorithm used to extrapolate functions and it is able to extend the valid region of the calculated far-field pattern up to the whole forward hemisphere. To verify the effectiveness of the method, several examples are presented using both simulated and measured truncated near-field data.**

I. INTRODUCTION

Truncation errors are always present in planar near-field (PNF) and cylindrical near-field (CNF) measurements, but not in SNF measurements, so the presence of this error depends only on the kind of acquisition surface. If the antenna under test (AUT) is fully enclosed by the acquisition surface, there are not truncation errors. In PNF and CNF measurements, due to the finite size of the scan area, the last condition is never fulfilled, and therefore, the far-field pattern is never known in the whole forward hemisphere. Normally, since the truncation error is an unavoidable error in PNF and CNF measurements and it is not present in SNF measurements, most of the approaches to reduce this kind of error have been specifically proposed for the two first configurations. An improvement of the far-field within the so-called reliable region or valid region (spectral region where the calculated far-field pattern is considered valid because the error introduced by the truncation is low) can be obtained by applying to the near-field data a proper window [1]-[2]. In [3]-[4], a method based on the determination of the equivalent currents on the AUT aperture by solving a system of integral equations is proposed. After that, the far-field is obtained in the whole space. Another approach [5] uses a singular value decomposition to extrapolate the near-field data outside the scan area. A recent publication [6] uses *a priori* information about the AUT in an iterative algorithm to extrapolate the far-field outside the reliable region. The theoretical basis of this iterative algorithm was presented in [7]-[8] by Gerchberg and Papoulis, respectively.

As it is well-known, the most accurate antenna patterns are obtained using the spherical near-field (SNF) technique not only because the measurement is performed in a controlled environment, but also because the antenna under test (AUT) is fully enclosed by the acquisition surface [9]. Therefore, truncation errors do not appear in this kind of measurement and the far-field pattern can be found in all directions. However, there are special cases, for example, when measuring electrically large antennas, where the measurement time with the SNF technique is prohibitively long and an acquisition over the whole spherical surface is not practical. Therefore, to reduce the data acquisition time, partial sphere measurement is usually made, taking samples over a portion of the spherical surface in the direction of the main beam. But in this case, the AUT radiation pattern is not known outside the measured angular sector as well as a truncation error is present in the calculated far-field pattern within this sector.

Although truncation error is only a typical error in PNF and CNF measurements, and therefore, most of the bibliography is focused on these kinds of configurations, there are also some studies to reduce the truncation error when measuring on a portion of a spherical surface. In [10], the truncated spherical near-field data are used to calculate an equivalent currents distribution of a set of dipoles that reproduce the radiation of the AUT. As in [3]-[4], once that distribution is known, the far-field can be easily computed in the whole sphere. In [11]-[12] an approach based on the Gerchberg-Papoulis iterative algorithm to extrapolate the far-field outside the reliable region is proposed. The main differences compared to the approach given in [6] are the domains where the successive projections are performed. In [11]-[12], the SNF acquisition and the spherical wave coefficients are used instead of employing the field distribution over the AUT and the plane wave spectrum (PWS) as in [6].

In the present work, a new method to extend the valid region of the calculated far-field up to the whole forward

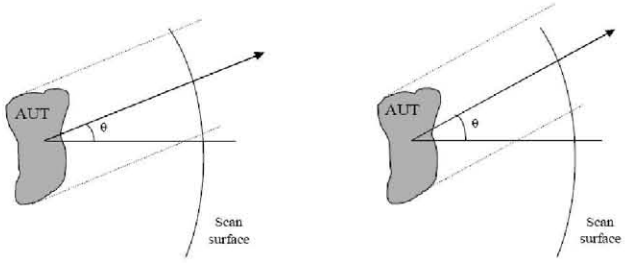

Fig. 1. Geometrical optics employed to define the theoretical reliable region. (a) Direction included in the reliable region. (b) Direction not included in the reliable region.

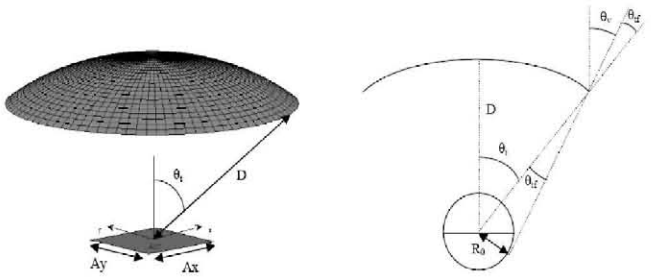

Fig. 2. Spherical near-field measurement setup with polar truncation.

hemisphere from a truncated SNF measurement is presented. This method uses an approach similar to that presented in [6]. However, since the initial data are not taken over the same surface, some differences have to be pointed out. First, the region where the calculated far-field pattern can be considered reliable will be different. Second, the iterative algorithm uses the PWS information over a regular kx-ky grid, which in the considered is obtained in a different way.

The paper is organized as follows. Section II defines the spectral region where the calculated far-field pattern can be considered theoretically reliable when measuring over a truncated sphere. The method to reduce truncation errors is described in section III. Section IV presents the simulated model which is used in Section V to analyze some critical aspects of the method. Section VI validates the method by using both simulated and measured near-field data. Conclusions are drawn in Section VII.

II. Theoretical Reliable Region

One important requirement in the proposed iterative method is the determination of a spectral region where the error in the calculated far-field pattern is zero, because the method only converges to the correct solution [8] when starting from data without errors. However, the whole calculated far-field pattern is always affected by errors and it is not possible to define a region where the error is completely zero. Therefore, we will use the concept of reliable region to refer to the spectral region where the error in the calculated far-field pattern is not negligible, but very low. A classical definition of an appropriate region is given in [9], [13], where geometrical optics is employed to calculate the maximum validity angles which are used to define a theoretical reliable region. With this definition, one particular direction will be within that reliable region when the scan surface includes all rays parallel to that direction coming from any part of the AUT (see Fig. 1 (a)). The opposite situation is shown in Fig. 1 (b), where there are rays that do not lie on the scan surface.

The theoretical reliable region for the PNF case is always the intersection of two orthogonal ellipses as was deduced in [6]. In the SNF case, it is possible to sample over different parts of the sphere, therefore, there will be different kinds of theoretical reliable regions, not as in the previous case where the shape of the reliable region was fixed. The choice of the sampling region will depend on the expected radiation pattern because the proposed method works better when most of the radiated energy is within that region. Therefore, the sampling region has to be the region where the main lobe is located. In this work, only the polar truncation is considered. This kind of truncation is carried out in elevation (measuring from $\theta=0^\circ$ up to a fixed value of θ) and it is the best choice when the AUT is steering at boresight. The analysis for any other kind of spherical truncation can be performed in a similar way.

According to geometrical optics (see Fig. 2), the maximum validity angle in elevation is given by

$$\theta_v = \theta_t - \theta_{tf} = \theta_t - \arcsin\left(\frac{R_0}{D}\right) \qquad (1)$$

where θ_v is maximum validity angle in elevation, θ_t represents the truncation angle, R_0 is the radius of the minimum sphere and D stands for the measurement distance.

Unlike the PNF case, now the maximum validity angle in elevation does not change for different azimuthal directions, and therefore, the theoretical reliable region is a circle within the circle that represents the whole visible region. This spectral region is mathematically represented by (2).

$$k_x^2 + k_y^2 < \left(k \sin\theta_v\right)^2 \qquad (2)$$

where k_x and k_y are the wavenumbers in the x and y directions, respectively.

III. Description of the Method

As commented before, when we perform a near-field measurement over an acquisition surface that does not fully enclose the AUT, a truncation error appears in the calculated far-field pattern. As a consequence, there is an angular region where that pattern is unknown. In some cases, this truncation is unavoidable (PNF and CNF measurements) and in other cases, (partial SNF measurements) it is deliberately introduced in order to reduce the measurement time. In this section, we present a method that can be applied in all cases to extrapolate the

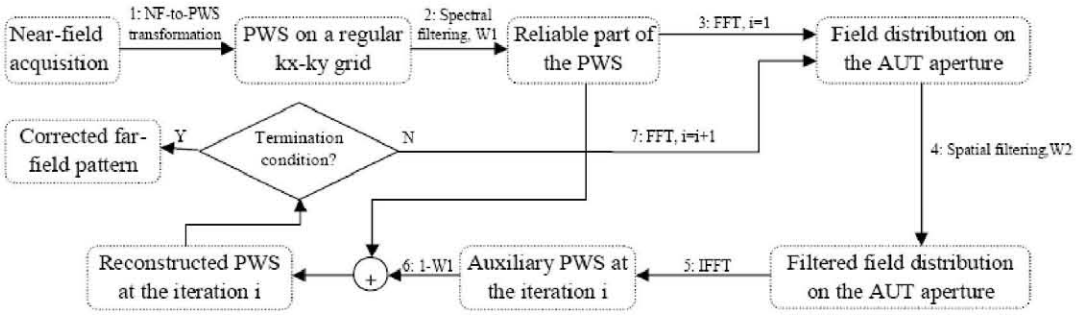

Fig. 3. Schematic diagram of the method to reduce truncation errors.

far-field pattern up to the whole forward hemisphere. This method is based on the iterative algorithm proposed in [7]-[8] and it has been already applied to the PNF case in [6]. However, taking into account some considerations, the method can be employed to reduce truncation errors in all kind of measurement configurations and particularly in partial SNF measurements. A generic schematic diagram of the method is shown in Fig. 3 and the steps are described in the following.

Step 1: The plane wave spectrum (PWS) is calculated from the near-field acquisition on a regular kx-ky grid. In the PNF case, the far-field is directly obtained in this kind of grid by calculating the Fourier Transform of the samples. In the SNF case, some modifications are needed because classical programs that perform a SNF-to-far-field transformation produce the final results on a regular θ-ϕ grid. The possibilities are:

a) The spherical wave coefficients are calculated and the far-field pattern functions [9] are evaluated in the desired angular directions defined by the regular kx-ky grid. Finally, the far-field is obtained in those directions

$$\vec{E}_{FF}(\theta,\phi) = C\sum_{smn} Q^{(3)}_{smn}\vec{K}(\theta,\phi) \tag{3}$$

b) The spherical wave coefficients are calculated and a SWE-to-PWE transformation [14] is applied.

$$\vec{T}(k_x,k_y,z) = \sum_{n=1}^{\infty}\sum_{m=-n}^{n} Q^{(3)}_{1mn}\vec{T}_{1mn}(k_x,k_y,z) + Q^{(3)}_{2mn}\vec{T}_{2mn}(k_x,k_y,z) \tag{4}$$

c) The far-field pattern is determined on a regular θ-ϕ grid by applying a SNF-to-far-field transformation. Then, the far-field is obtained on a regular kx-ky grid by interpolating the previous information.

Step 2: The unreliable portion of the PWS is filtered out by using the spectral window defined in (2).

Step 3: A field distribution over the AUT plane is obtained by taking the Fourier Transform of the filtered PWS.

Step 4: The previous field distribution is spatially filtered taking into account that the field outside the AUT aperture is theoretically zero.

Step 5: The filtered field distribution is Fourier transformed back to the spectral domain.

Step 6: A new PWS is calculated by substituting the unreliable portion of the initial PWS for same portion of the PWS obtained in the previous step.

Step 7: If the new PWS fulfills the termination condition, the algorithm stops. If not, a new iteration starting from the step 4 is carried out.

IV. Simulated Model

In the following sections, several results will be presented in order to analyze and validate the proposed method. The input data used to obtain those results are simulated SNF data. The AUT employed in the simulation is a square aperture with a gaussian-tapered field distribution as (5) shows.

$$\vec{E}_G = E_0 e^{-\left(\frac{x^2}{2\sigma_x^2}+\frac{y^2}{2\sigma_y^2}\right)}\hat{x};\quad \vec{H}_G = \frac{1}{\eta}\hat{z}\times\vec{E}_G \tag{5}$$

The aperture size was 8λ×8λ, the measurement distance was 30λ and the samples were taken each degree both in θ and ϕ. Two simulations were carried out. In the first one, we used the whole sphere as scan surface in order to obtain the reference pattern. In the second simulation, a truncation angle in elevation equal to 20º was employed.

V. Critical Aspects of the Method

All steps of the proposed method were indicated in Section III, however, some remarks are required. First, we need to concrete the kind of spectral filtering which is applied. Second, the termination condition has to be described.

As deduced from [8], when starting from exact data, the method converges to the correct solution. Otherwise, the error decreases with the iteration number, but after several iterations it starts increasing. In Section II, the definition for

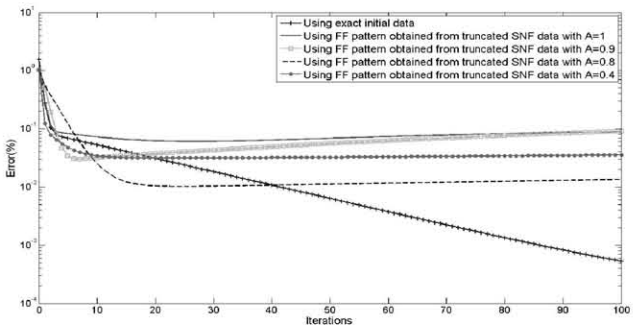

Fig. 4. Error as a function of the iteration number using different reliable regions.

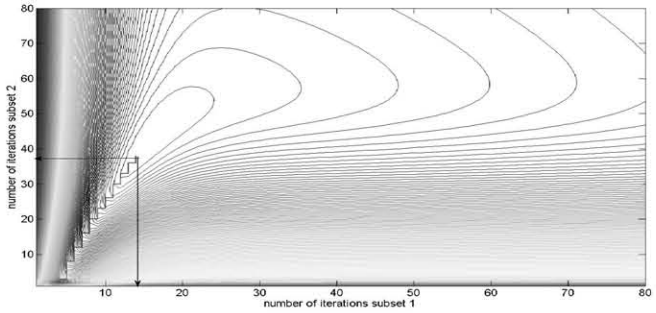

Fig. 5. Gradient Descent algorithm employed to search the minimum.

the theoretical reliable region was presented. However, the error within that region may be relatively high. Therefore, we will not reach a very low error in the reconstructed pattern, as shown by the red line in Fig. 4. Logically, the convergence of the iterative method will be better if we use an initial spectral region where the error is lower. Intuitively, one easy way to achieve this is to employ a spectral region smaller than the theoretical reliable region. The angle that defines this new region can be expressed as a function of the maximum validity angle obtained in (1).

$$\theta_v^{'} = \theta_v \cdot A = \left(\theta_t - \arcsin\left(\frac{R_0}{D}\right)\right) \cdot A \qquad (6)$$

As observed in Fig. 4, when the chosen region is smaller (A<1), the minimum error achieved with the method is lower. However, when that region is smaller than a certain size, the behavior is just the opposite, i.e., the minimum error increases. In general, a value of A between 0.4 and 0.8 will give us a low error in the final radiation pattern.

The error in the reconstructed far-field pattern will not decrease monotonically with the iteration number, but as observed in Fig. 4, there is a minimum that can be used as termination point. An algorithm to find that minimum was proposed in [6] and it is based on the following principle: if we use different initial truncated surfaces, the initial error within the reliable region will be also different and the error in the iterative procedure will vary in a different way. Therefore, when comparing the iterative results obtained in each case, we will have a minimum when both

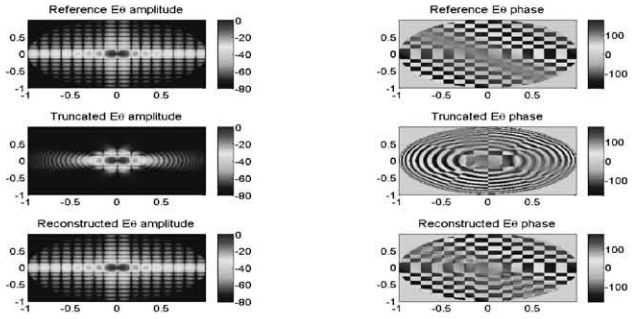

Fig. 6. Comparison between the θ-component of the reference, truncated and reconstructed far-field pattern (simulated model).

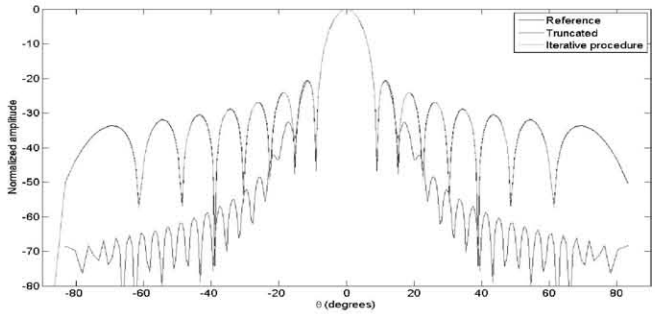

Fig. 7. Comparison between the reference, truncated and reconstructed co-polar far-field pattern for the ϕ = 0º cut (simulated model).

results have the minimum error. The main drawback of this proposal is that a lot of iterations and comparisons are required. To solve this problem, we propose here to use an optimization algorithm to find the minimum, e.g., the Gradient Descent algorithm. With this algorithm, we move always in one direction where the function decreases stopping when we reach the minimum, as shown Fig. 5.

VI. Numerical Results

After studying different critical parts of the proposed method, we present some results in order to validate it.

In the first example, the simulation results described in Section IV were employed. Since the antenna is steering at boresight, the most appropriate way to reduce the measurement time was a polar truncation, measuring from θ=0º to θ=20º. The iterative method was applied using a value of A equal to 0.8 and the second subset employed in the algorithm to find the termination point was obtained from the simulated data by removing the information located from θ=17º to θ=20º. Fig. 6 shows the θ-component (in amplitude and phase) of the reference, truncated and reconstructed far-field pattern in the first, second and third row, respectively. The cut ϕ = 0º of the far-field pattern is depicted in Fig. 7, where it is possible to appreciate better the very good agreement between the reference and the reconstructed pattern.

In the second validation, data from an actual measurement were used. The measurement was performed in the spherical-range measurement system in the anechoic chamber at the

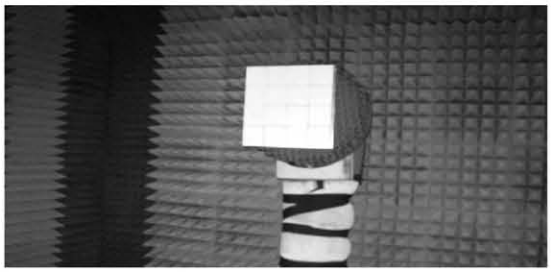

Fig 8. Measurement of an X-Band array antenna in spherical near-field.

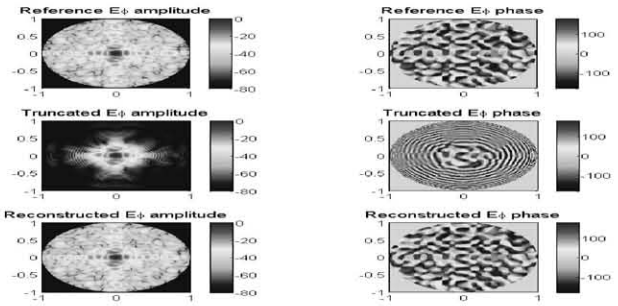

Fig. 9. Comparison between the ϕ-component of the reference, truncated and reconstructed far-field pattern (X-Band array antenna).

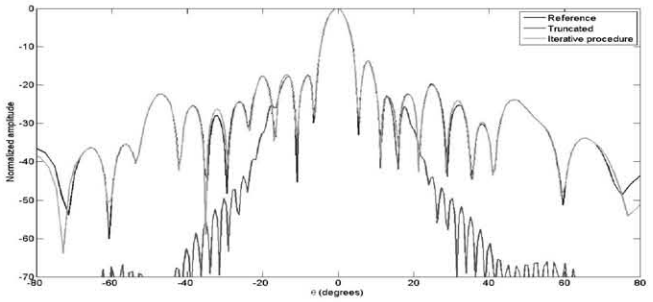

Fig. 10. Comparison between the reference, truncated and reconstructed co-polar far-field pattern for the $\phi = 0^{\circ}$ cut (X-Band array antenna).

Technical University of Madrid (UPM). The AUT is formed by a square array of 256 printed elements covering a large bandwidth at X-Band and its dimensions are 40×40 cm. The array is divided into 16 square subarrays of 4x4 elements (see Fig. 8). Data in the whole sphere were taken, but only information from $\theta=0^{\circ}$ to $\theta=20^{\circ}$ was used as input data to the method. After applying the iterative procedure, we obtain the results shown in Fig. 9 and Fig. 10.

VII. Conclusions

A method to reduce truncation errors in partial SNF measurements has been proposed. The method is based on an iterative algorithm to extrapolate functions. Moreover, the effect of the size of the spectral region taken as reliable region in the method has been investigated. After defining the most appropriate size for this region, an algorithm to find the optimum termination point has been presented. The method has been validated by using both simulated and measured near-field data, showing that it is possible to reduce very effectively the truncation errors. It was noted that the proposed method works very well for the planar aperture antennas, like large antenna arrays, because the antenna aperture, were the fields are theoretically concentrated, is well defined.

Acknowledgment

This work has been developed thanks to the Spanish FPU grant for Ph.D. students and the financing of the Crocante Project (TEC2008-06736-C03-01/TEC). F. J. Cano-Fácila would also like to thank DTU Electrical Engineering for the support during his stay at the Technical University of Denmark.

References

[1] P. R. Rousseau, "The planar near-field measurement of a broad beam antenna using a syntethic subarray approach," in *IEEE AP-S Symp. Digest*, 1997, pp. 160-163.

[2] E. B. Joy, "Windows '96 for planar near-field measurements," in *AMTA Proc.*, 1996, pp. 80-85.

[3] P. Petre and T. K. Sarkar, "Planar near-field to far-field transformation using an equivalent magnetic current approach," *IEEE Trans. Antennas Propag.*, vol. 40, pp. 1348-1356, Nov. 1992.

[4] J. Perez and J. Baserrechea, "Analysis of different GA strategies applied to antenna far-fields reconstruction from planar acquisition," *Microw. Opt. Tech. Lett.*, vol. 39, pp. 422-426, 2003.

[5] O. M. Bucci, G. D. D'Elia, and M. D. Migliore, "A new strategy to reduce truncation error in near-field/far-field transformations," *Radio Sci.*, vol. 35, pp. 3-17, 2000.

[6] E. Martini, O. Breinbjerg, and S. Maci, "Reduction of truncation errors in planar near-field aperture antenna measurements using the Gerchberg-Papoulis algorithm," *IEEE Trans. Antennas Propagat.*, vol. 56, no. 11, pp. 3485-3493, Nov., 2008.

[7] R. W. Gerchberg, "Super-resolution through error energy reduction," *Opti. Acta*, vol. 21, no. 9, pp. 709-720, May 1974.

[8] A. Papoulis, "A new algorithm in spectral analysis and bandlimited extrapolation," *IEEE Trans. Circuits Syst.*, vol. CAS-22, no. 9, pp-735-742, Sep 1975.

[9] J. E. Hansen (Ed.), *Spherical Near-field Antenna measurements*. Peter Peregrinus Ltd., London, U.K., 1988.

[10] M. Serhir, J-M. Geffrin, A. Litman, and P. Besnier, "Aperture antenna modeling by a finite number of elemental dipoles from spherical field measurements," *IEEE Trans. Antennas Propagat.*, vol. 58, no. 4, pp. 1260-1268, Apr., 2010.

[11] A. Clemente, " Reduction of truncation errors in spherical near-field antenna measurements," Master's thesis at Technical University of Denmark, DTU Electrical Engineering, Departament of Electrical Engineering, May 2009.

[12] E. Martini, S. Macci, and L. Foged, "Reduction of truncation errors in spherical near-field measurements," in *AMTA Proc.*, 2010, Atlanta.

[13] A. D. Yaghjian, "Upper bound errors in far-field antenna parameters determined from planar near-field measurements," Nat. Bur. Stand., Boulder, CO, Tech. Rep. NBS Tech. Notes 667, 1975.

[14] C. Cappellin, " Antenna Diagnostic for spherical near-field antenna measurements," Ph.D Thesis at Technical University of Denmark, DTU Electrical Engineering, Departament of Electrical Engineering, Sep. 2007.